All-Optical Control of Gigahertz Acoustic Resonances by Forward Stimulated Interpolarization Scattering in a Photonic Crystal Fiber

M. S. Kang,* A. Brenn,* and P. St.J. Russell*

Max-Planck Institute for the Science of Light, Guenther-Scharowsky-Strasse 1/Bau 24, 91058 Erlangen, Germany

(Received 1 July 2010; revised manuscript received 27 August 2010; published 5 October 2010)

We report the observation of a novel nonlinear optoacoustic phenomenon, that we name forward stimulated interpolarization scattering. When two frequency-offset laser signals are colaunched into orthogonally polarized guided modes of a birefringent small-core (1.8 μm diameter) photonic crystal fiber, a pattern of axially moving polarization fringes is produced, with a velocity and spacing that depends on the frequency offset. At values of frequency offset in the few-GHz range, the pattern of moving fringes can perfectly match the phase velocity and axial wavelength (3.9 mm) of the torsional-radial acoustic mode tightly guided in the core. An intense optoacoustic interaction ensues, leading to efficient nonlinear exchange of power from the higher frequency (pump) mode to the orthogonally polarized lower frequency (Stokes) mode. A full-vectorial theory is developed to explain the observations.

DOI: 10.1103/PhysRevLett.105.153901 PACS numbers: 42.81.−i, 42.65.Es, 42.65.Wi, 43.35.Sx

Tight confinement of both acoustic vibrations and light in a small space can give rise to strong interactions between them, yielding new nonlinear optical phenomena. One recent example is forward stimulated Raman-like scattering (SRLS) in an air-silica photonic crystal fiber (PCF) with a micron-sized glass core surrounded by a hexagonal array of hollow channels [1]. Radially "breathing" acoustic resonances (ARs) transversely trapped in the tiny core can act as highly efficient Raman-like oscillators, mediating the SRLS process. When copolarized pump (frequency f_P) and Stokes (frequency f_S) waves are launched together into the PCF, their frequency difference being tuned to the AR frequency ($f_{AR} = f_P - f_S$), a coherent AR is efficiently generated via electrostriction, which in turn transfers power from pump to Stokes. As the optical power is increased, a comb of higher-order Stokes and anti-Stokes waves is generated with frequency spacing f_{AR} via cascaded coherent Stokes and anti-Stokes scattering. While the simultaneous generation of many sidebands can be useful in applications such as frequency comb generation, pulse synthesis, and laser mode-locking, in signal processing applications it is important to be able to separate out an individual sideband. This is not straightforward to achieve, however, because all the SRLS sidebands are in the same optical mode and spectrally very close to each other with typically a few-GHz spacing.

In this Letter, we report the first demonstration of what we call "forward stimulated interpolarization scattering" (SIPS). In the experiment, copropagating pump and Stokes waves are launched into orthogonally polarized eigenmodes of a weakly birefringent PCF. These cause a coherent torsional-radial (TR) "squeezing" AR to be efficiently excited in the fiber core, which then couples power from pump to Stokes. The two orthogonally polarized signals can be simply separated at any arbitrary wavelength using a polarizing beam splitter, thus overcoming the SRLS signal-separation problem. We also show that, in contrast to SRLS, coherent Stokes and anti-Stokes scattering is highly suppressed in the SIPS process, because the driven AR is not phase matched to the higher-order Stokes and anti-Stokes waves. A rigorous vectorial theory is developed to describe both SIPS and SRLS.

Figure 1 shows the dispersion diagrams for the optical and acoustic modes, comparing forward SIPS and SRLS. In the case of SIPS [Fig. 1(a)], the pump and Stokes waves are either in the slow and fast optical modes, or vice versa. The two configurations of SIPS have the same acoustic frequency, which is independent of the pump frequency because the acoustic dispersion is almost flat around the phase-matching points. In this sense, SIPS may also be considered Raman-like [2]. In contrast to SRLS [Fig. 1(b)], however, the driven AR does not have the correct axial wave vector to cause scattering into higher-order Stokes and anti-Stokes waves, for either of the two situations. Therefore, the SIPS process transfers pump power only to the Stokes wave, generation of higher-order sidebands being highly suppressed. This is similar to the case of conventional (backward) stimulated Brillouin scattering (SBS).

In a circularly symmetric cylindrical rod, each TR_{2m} acoustic branch has two degenerate modes, one vibrating with squeezing orientation along the 0°/90° axes, and the other along 45°/−45° axes [3], as shown below the dispersion diagrams in Fig. 1. Considering the symmetry of the HE_{11} optical mode and the TR_{2m}-AR, it can be shown that the TR_{2m}-AR oriented along the 45°/−45° axes can mediate only forward SIPS, while the TR_{2m}-AR along the 0°/90° axes can cause only forward SRLS. This will be discussed in more detail later.

We investigate experimentally both forward SIPS and SRLS in a PCF using the setup shown in Fig. 2. The output of a single-frequency external-cavity diode laser oscillating

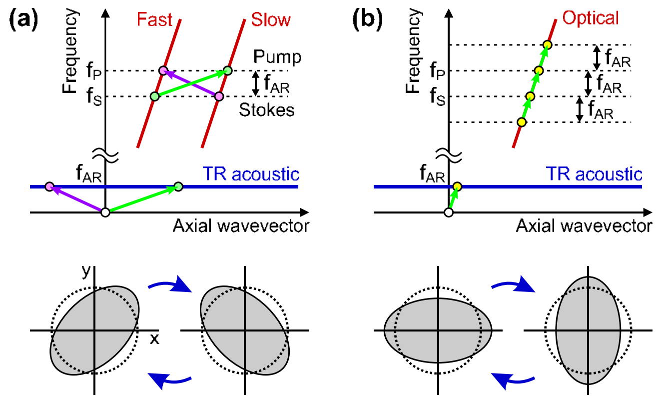

FIG. 1 (color online). Dispersion diagrams (not to scale) for the optical modes and the TR acoustic mode, comparing SIPS (a) and SRLS (b). The orientations of the TR-AR displacements causing SIPS and SRLS are also shown below the corresponding dispersion diagrams, where the dotted circles and the gray ellipses represent the original core and the vibrating one. The horizontal and vertical lines correspond to the fiber eigenaxes (x and y). In (a), two different colors (green and violet) of the circles and arrows in the dispersion diagram correspond to two configurations of SIPS. In (b), the optical mode can be either the fast or the slow mode.

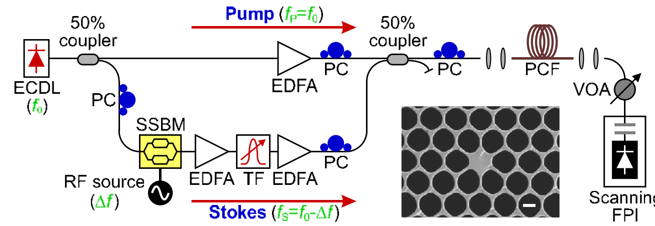

FIG. 2 (color online). Schematic diagram of the experimental setup. ECDL: external-cavity diode laser, PC: polarization controller, SSBM: single-sideband modulator, EDFA: erbium-doped fiber amplifier, TF: tunable filter, VOA: variable optical attenuator, FPI: Fabry-Pérot interferometer. The inset is a scanning electron micrograph of the PCF used in the experiment. The white horizontal bar corresponds to 1 μm.

at 1550 nm is split into two waves at a 50:50 fiber coupler. One of these waves plays the role of a pump wave. The other is frequency-down-shifted by an electro-optic single-sideband modulator, and acts as the Stokes wave. The polarization state and optical power of the two waves are controlled independently by adjusting the polarization controller and the Er-doped fiber amplifier in each optical path. The two waves are then combined at a second 50:50 fiber coupler and launched into the PCF. The spectrum of the transmitted light from the PCF is measured using a scanning Fabry-Pérot interferometer.

In the experiment, we used a 15 m length of highly nonlinear air-silica PCF with 1.8 μm core diameter (the inset of Fig. 2). We characterized the ARs in the fiber core by pump-probe measurements using a Sagnac interferometer [4]. The frequencies of the TR_{21}-like and R_{01}-like ARs were 1.50 and 1.80 GHz. The fiber was polarization maintaining with a beat length of 3.9 mm (corresponding to a birefringence of 4.0×10^{-4}), measured by scanning a point force along the fiber and monitoring the polarization state at the output [5]. This birefringence is attributed to deviations from ideal sixfold symmetry of the microstructure around the core [6,7].

We investigated the characteristics of forward SIPS and SRLS mediated by the TR_{21}-like AR. First, pump and Stokes waves each with an optical power of 42 mW were launched and the power conversion from the pump to Stokes measured as the frequency difference was tuned around the measured AR frequency of 1.50 GHz. Both SIPS and SRLS were observed, with Lorentzian-like gain profiles of linewidth 7 MHz, as shown in Fig. 3(a). Furthermore, for both scattering processes almost the same result was obtained no matter whether the pump or Stokes waves were polarized along the fast or slow or the slow or fast fiber axes. The SIPS and SRLS resonant acoustic frequency and peak gain coefficient were, however, slightly different, SIPS showing a gain of 1.0 $m^{-1} W^{-1}$ at 1.5015 GHz, compared to 0.65 $m^{-1} W^{-1}$ at 1.497 GHz for SRLS. We attribute this to acoustic birefringence caused by structural deformations around the core, which can break the twofold degeneracy of each TR acoustic branch [3]. One might perhaps attribute the difference in resonant frequency to a difference in phase-matching acoustic wave vector between SIPS and SRLS (the acoustic wavelength is 3.9 mm for SIPS and 15 cm for SRLS); however, the acoustic dispersion is very flat at these very small wavevector values (Fig. 1), giving rise to an acoustic frequency difference of only 200 Hz, not 4.5 MHz as measured. We also monitored the Stokes power conversion as a function of launched optical power, equally split between pump and Stokes waves. In SIPS the conversion saturates with increasing power, while in SRLS the pump wave recovers after full depletion [1], as shown in Fig. 3(b). The measured power dependences agree well with an analytical theory for both scattering processes, to be presented in a later section. At a total input power of 300 mW, ~97% of the pump power was transferred to the Stokes in SIPS [Fig. 3(c)]. As mentioned above, higher-order Stokes and anti-Stokes waves were not generated, in contrast to the case of SRLS [Fig. 3(d)].

We also examined the properties of forward SIPS and SRLS mediated by the radial R_{01}-like AR. This AR caused only SRLS as reported in [1], while SIPS could hardly be observed, as shown in Fig. 4(a). The fiber had a 15 MHz wide SRLS gain profile with a peak gain of 1.0 $m^{-1} W^{-1}$. Anti-Stokes and second-order Stokes waves, created via coherent anti-Stokes and Stokes scattering, are clearly seen in the output spectrum in Fig. 4(b).

We now theoretically analyze both forward SIPS and SRLS using an approach that takes full account of the vectorial nature of both the electromagnetic and the acoustic fields. Theories that treat density variations alone [1,8] cannot either explain SIPS or yield a quantitatively rigorous

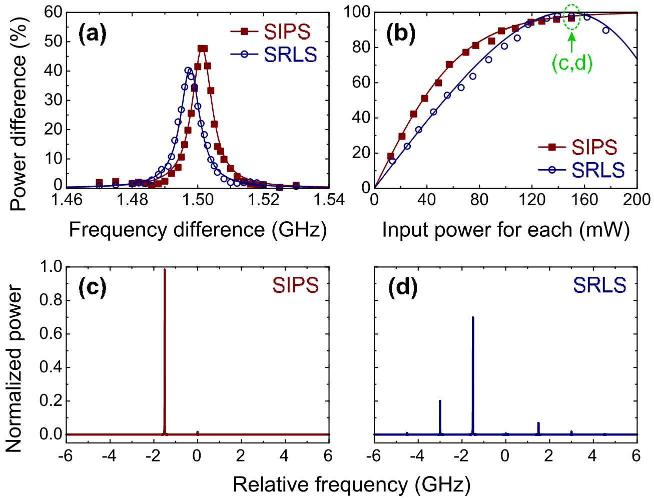

FIG. 3 (color online). (a),(b) Power conversion from pump to Stokes as a function of (a) frequency difference ($f_P - f_S$) around the TR_{21}-like AR frequency at 1.50 GHz, and (b) input power of each wave ($P_{P0} = P_{S0}$). The vertical axes represent the relative difference of output power between the pump and Stokes waves. The dots are experimental results and the lines are fits to the analytical theory. In (a), the input power of each wave is fixed at 42 mW. In (b), the frequency difference is tuned to the resonant frequency for each case, i.e., 1.5015 GHz for SIPS and 1.497 GHz for SRLS. (c),(d) Output spectra at a total input power of 2 × 150 mW for SIPS (c) and SRLS (d). These spectra correspond to the two points indicated by the green dashed circle in (b). Zero relative frequency corresponds to the pump wave.

analysis of SRLS. Let us first consider the case of SIPS, where only two optical waves are involved in the scattering process and the generation of higher-order sidebands is strongly suppressed. The total electric field in the fiber can then be written

$$\mathbf{E}(\mathbf{r}, z, t) = \mathbf{E}_P(\mathbf{r}, z, t) + \mathbf{E}_S(\mathbf{r}, z, t),$$
$$\mathbf{E}_k(\mathbf{r}, z, t) = \mathbf{E}_{k0}(\mathbf{r}) a_k(z, t) e^{i(\beta_k z - \omega_k t)} + \text{c.c.}, \quad (1)$$

where $k = P, S$ denote pump and Stokes waves. For SIPS, the normalized electric field distributions $\mathbf{E}_{k0}$ become $\mathbf{E}_{P0} = \mathbf{E}_{x0}$ and $\mathbf{E}_{S0} = \mathbf{E}_{y0}$, or vice versa, where $\mathbf{E}_{x0}$ and $\mathbf{E}_{y0}$ represent x- and y-polarized fundamental optical modes. The slowly varying field amplitudes are a_k, the axial wave vectors β_k, and the angular frequencies ω_k. Polarization beating between the two waves drives, via electrostriction, a coherent AR with axial wave vector $q = \beta_P - \beta_S$ and angular frequency $\Omega = \omega_P - \omega_S$. This AR is governed by the acoustic wave equation for the displacement vector $\mathbf{u}(\mathbf{r}, z, t)$ [9–11]:

$$\frac{\partial^2 \mathbf{u}}{\partial t^2} + \Gamma \frac{\partial \mathbf{u}}{\partial t} + V_S^2 \nabla \times (\nabla \times \mathbf{u}) - V_L^2 \nabla(\nabla \cdot \mathbf{u}) = \frac{\mathbf{F}}{\rho_0},$$
$$\mathbf{F} = \varepsilon_0 \left[\frac{1}{2} \gamma_{12} \nabla(\mathbf{E} \cdot \mathbf{E}) + \gamma_{44} (\mathbf{E} \cdot \nabla) \mathbf{E} \right], \quad (2)$$

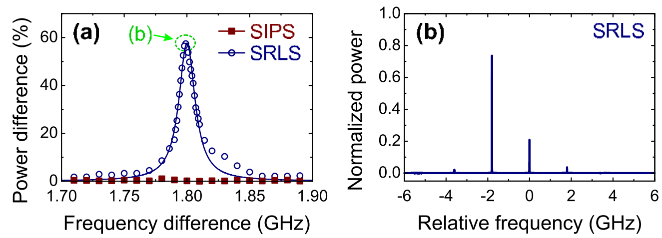

FIG. 4 (color online). (a) Power conversion from pump to Stokes as a function of frequency difference ($f_P - f_S$) around the R_{01}-like AR frequency at 1.80 GHz. The input power of each wave is fixed at 42 mW. Dots are experimental results and the curve is a fit assuming a Lorentzian gain profile. (b) Output spectrum for SRLS corresponding to the point indicated by the green dashed circle in (a).

where Γ, V_S, V_L, and ρ_0 are the acoustic damping rate, shear sound velocity, longitudinal sound velocity, and density of fused silica. $\mathbf{F}$ is the electrostrictive driving term (EDT), ε_0 is the electric permittivity in vacuum, and γ_{12} and γ_{44} are the elements of the electrostrictive tensor for fused silica. We are interested in the case where the EDT strongly drives a specific AR (e.g., the TR_{21}-like AR). The displacement vector of this driven AR can then be written $\mathbf{u}(\mathbf{r}, z, t) = \mathbf{u}_m(\mathbf{r}) b(z, t) e^{i(qz - \Omega t)} + \text{c.c.}$, where $b(z, t)$ is its slowly varying acoustic amplitude and $\mathbf{u}_m(\mathbf{r})$ is the normalized displacement distribution, which is a solution of Eq. (2) for $q = q_m$ and $\Omega = \Omega_m$ in the absence of acoustic damping ($\Gamma = 0$) or any EDT ($\mathbf{F} = 0$). The driven AR produces a nonlinear polarization expressed as [9–11]

$$\mathbf{P}^{\rm NL} = -\varepsilon_0 [\gamma_{12} (\nabla \cdot \mathbf{u}) \mathbf{E} + 2\gamma_{44} (\nabla_S \mathbf{u}) \cdot \mathbf{E}], \quad (3)$$

where $\nabla_S \mathbf{u} \equiv [\nabla \mathbf{u} + (\nabla \mathbf{u})^T]/2$. The nonlinear polarization $\mathbf{P}_k^{\rm NL}$ for each optical wave is derived by extracting relevant terms from the total nonlinear polarization $\mathbf{P}^{\rm NL}$ and then included as a driving term in the optical wave equation:

$$\nabla^2 \mathbf{E}_k - \frac{n_k^2}{c^2} \frac{\partial^2 \mathbf{E}_k}{\partial t^2} = \frac{1}{\varepsilon_0 c^2} \frac{\partial^2 \mathbf{P}_k^{\rm NL}}{\partial t^2}, \qquad (k = P, S), \quad (4)$$

where c is the speed of light in vacuum and n_k the effective refractive index of each optical wave. After some manipulation of the coupled-wave equations in Eq. (4), we obtain the evolution of optical power in pump and Stokes waves:

$$P_P(z) = P_{\rm in} \frac{P_{P0}}{P_{P0} + P_{S0} \exp(g P_{\rm in} z)},$$
$$P_S(z) = P_{\rm in} \frac{P_{S0}}{P_{S0} + P_{P0} \exp(-g P_{\rm in} z)},$$
$$g(\Omega - \Omega_m) = g_0 \frac{(\Gamma/2)^2}{(\Omega - \Omega_m)^2 + (\Gamma/2)^2}, \quad (5)$$
$$g_0 = -\frac{\omega_0 (\gamma_{12} Q_1 + 2\gamma_{44} Q_2)(\gamma_{12} R_1 + 2\gamma_{44} R_2)}{2 n_x n_y c^2 \rho_0 \Omega_m \Gamma},$$

where $P_{k0} \equiv P_k(z = 0)$ is the input power of each wave, $P_{in} \equiv P_{P0} + P_{S0}$ is the total input power, and the optical power is expressed via $P_k = 2n_k \varepsilon_0 c|a_k|^2$ [12]. The gain profile is Lorentzian with linewidth Γ and peak gain coefficient g_0. Q and R are optoacoustic overlap integrals, defined in the case of SIPS as

$$\begin{aligned} Q_1 &= \int \mathbf{u}_m \cdot \nabla(\mathbf{E}_{x0} \cdot \mathbf{E}^*_{y0}) dA, \\ Q_2 &= \frac{1}{2} \int \mathbf{u}_m \cdot \{(\mathbf{E}_{x0} \cdot \nabla^*_{\beta_y})\mathbf{E}^*_{y0} + (\mathbf{E}^*_{y0} \cdot \nabla_{\beta_x})\mathbf{E}_{x0}\} dA, \\ R_1 &= \int (\nabla \cdot \mathbf{u}_m)(\mathbf{E}^*_{x0} \cdot \mathbf{E}_{y0}) dA, \\ R_2 &= \int \mathbf{E}^*_{x0} \cdot (\nabla_S \mathbf{u}_m) \cdot \mathbf{E}_{y0} dA. \end{aligned} \tag{6}$$

where $\nabla_\beta \equiv \nabla_\perp + i\beta\hat{\mathbf{z}}$ ($\nabla_\perp$: transverse gradient). We note that $(\gamma_{12}Q_1 + 2\gamma_{44}Q_2)(\gamma_{12}R_1 + 2\gamma_{44}R_2)$ is negative, so that g_0 is always a positive quantity.

In the case of SRLS, higher-order Stokes and anti-Stokes waves also play an important role in the scattering process. This means that all higher-order sidebands must be considered in general, although when $gP_{in}z \ll 1$ the generation of higher-order sidebands is not significant and the evolution of the two input waves closely resembles that of SIPS [Eq. (5)]. Since all the waves are in the same optical mode, the total electric field in the fiber in Eq. (1) can be modified as

$$\begin{aligned} \mathbf{E}(\mathbf{r}, z, t) &= \sum_k \mathbf{E}_k(\mathbf{r}, z, t), \quad k: \text{ integer}, \\ \mathbf{E}_k(\mathbf{r}, z, t) &= \mathbf{E}_0(\mathbf{r}) a_k(z, t) e^{i(\beta_k z - \omega_k t)} + \text{c.c.}, \end{aligned} \tag{7}$$

where $\omega_k = \omega_0 + k\Omega$, ω_0 being the angular frequency of the pump wave. It can be shown that Q and R take the same forms as Eq. (6) if $\mathbf{E}_{x,y0}$ is replaced with $\mathbf{E}_0$ and $\beta_{x,y}$ with $\beta_{0,-1}$. At resonance ($\Omega = \Omega_m$) the following analytical solutions can be derived:

$$\begin{aligned} P_k(z) = \Big[&\sqrt{P_{P0}} J_k(g_0\sqrt{P_{P0}P_{S0}}z) \\ &+ \sqrt{P_{S0}} J_{k+1}(g_0\sqrt{P_{P0}P_{S0}}z) \Big]^2, \end{aligned} \tag{8}$$

where J_k is the Bessel function of the first kind. We emphasize that these Bessel functions imply repeated depletion and recovery of each wave during propagation, while the exponential functions in Eq. (5) for SIPS indicate that the Stokes power conversion will saturate above a certain optical power level [Fig. 3(b)].

The gain factor g_0 may be estimated by approximating the fiber core as a cylindrical silica rod surrounded by air. Using $V_L = 5996$ m/s and $V_S = 3740$ m/s for fused silica, the measured acoustic frequency of the TR_{21}-like AR (1.50 GHz) corresponds to a rod radius of 0.93 μm [3]. We can readily obtain solutions for the optical modes ($\mathbf{E}_{x0}$, $\mathbf{E}_{y0}$, and β) and the acoustic displacement distribution ($\mathbf{u}_m$) in this rod, from which Q and R can be numerically calculated. Using $\gamma_{12} = 1.17$, $\gamma_{44} = -0.32$, $\rho_0 = 2.20 \times 10^{-3}$ kg/m^3 for fused silica and the experimental values $\omega_0/2\pi = 194$ THz, $\Omega_m/2\pi = 1.50$ GHz, and $\Gamma/2\pi = 7$ MHz, we estimate $g_0 = 1.1$ m^{-1} W^{-1} for forward SIPS and SRLS, which shows reasonably good agreement with measurement ($g_0 = 1.0$ m^{-1} W^{-1} for SIPS and $g_0 = 0.65$ m^{-1} W^{-1} for SRLS). It can be also shown analytically that $Q_1 = Q_2 = R_1 = R_2 = 0$ both for the 0°/90° TR_{21}-AR SIPS and for the 45°/−45° TR_{21}-AR SRLS; i.e., these scattering processes do not take place. In a similar manner, the gain factor for R_{01}-like AR SRLS at 1.80 GHz is estimated to be $g_0 = 1.8$ m^{-1} W^{-1}, while $Q_1 = Q_2 = R_1 = R_2 = 0$ analytically for SIPS, which is also in good agreement with the experimental results.

In conclusion, strong all-optical coupling between orthogonally polarized, frequency-offset, modes of a weakly birefringent solid-core PCF occurs when the frequency offset is tuned to match the frequency of a TR-like acoustic mode in the core. In contrast to SRLS, the characteristics of SIPS are similar to those of conventional backward SBS; i.e., only two waves (pump and Stokes) are phase matched and interact with the optically driven acoustic mode, prohibiting generation of higher-order Stokes and anti-Stokes waves. Since our experimental scheme allows independent control of pump and Stokes waves, it may also be possible to achieve forward stimulated scattering between two different spatial modes, e.g., scattering between the LP_{01} and LP_{11} optical modes mediated by a flexural acoustic vibration. Since the orthogonally polarized pump and Stokes waves can be simply separated regardless of their wavelength using a polarizing beam splitter, SIPS has practical advantages over SRLS in some applications, e.g., all-fiber optical amplifiers or attenuators, optical signal processing, and optical sensing.

*www.pcfiber.com

[1] M. S. Kang *et al.*, Nature Phys. **5**, 276 (2009).
[2] A. Brenn *et al.*, J. Opt. Soc. Am. B **26**, 1641 (2009).
[3] R. M. Shelby, M. D. Levenson, and P. W. Bayer, Phys. Rev. B **31**, 5244 (1985).
[4] M. S. Kang *et al.*, Appl. Phys. Lett. **93**, 131110 (2008).
[5] K. Takada, J. Noda, and R. Ulrich, Appl. Opt. **24**, 4387 (1985).
[6] J. C. Knight *et al.*, Opt. Lett. **21**, 1547 (1996).
[7] P. Dainese *et al.*, Opt. Express **14**, 4141 (2006).
[8] V. I. Kovalev and R. G. Harrison, Phys. Lett. A **374**, 2297 (2010).
[9] E. Peral and A. Yariv, IEEE J. Quantum Electron. **35**, 1185 (1999).
[10] A. S. Biryukov, M. E. Sukharev, and E. M. Dianov, Quantum Electron. **32**, 765 (2002).
[11] G. S. Wiederhecker *et al.*, Phys. Rev. Lett. **100**, 203903 (2008).
[12] R. W. Boyd, *Nonlinear Optics* (Academic Press, San Diego, 2008).